NACA

RESEARCH MEMORANDUM

PRELIMINARY SURVEY OF BOUNDARY-LAYER DEVELOPMENT

AT A NOMINAL MACH NUMBER OF 5.5

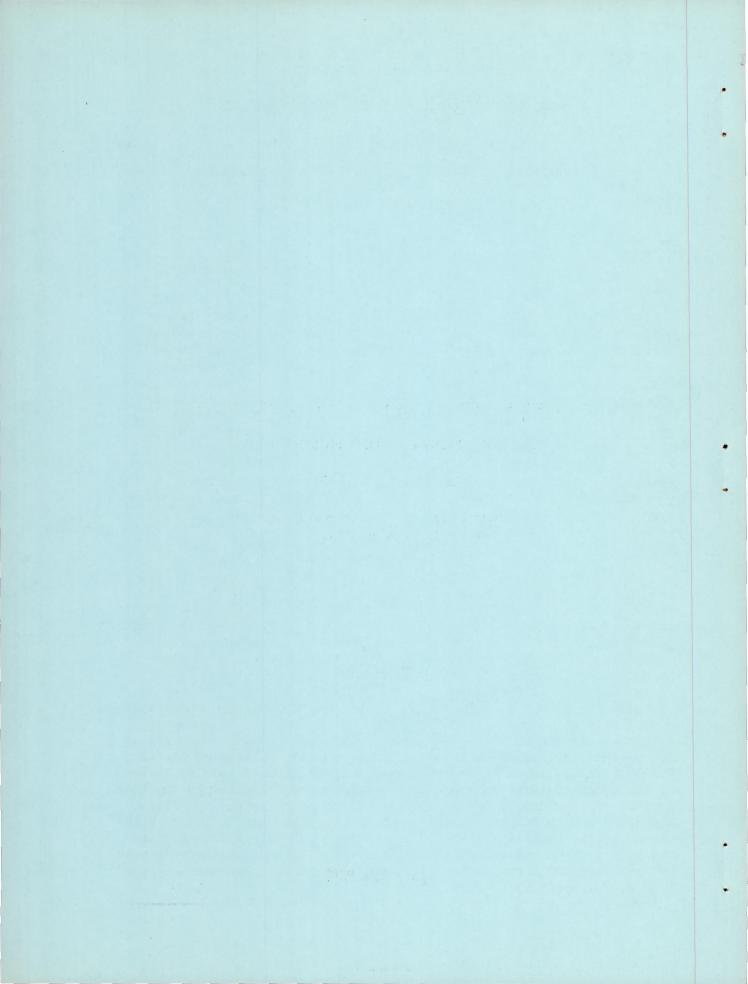
By Harold L. Bloom

Lewis Flight Propulsion Laboratory Cleveland, Ohio

NATIONAL ADVISORY COMMITTEE FOR AERONAUTICS

WASHINGTON

June 18, 1952



NATIONAL ADVISORY COMMITTEE FOR AERONAUTICS

RESEARCH MEMORANDUM

PRELIMINARY SURVEY OF BOUNDARY-LAYER DEVELOPMENT

AT A NOMINAL MACH NUMBER OF 5.5

By Harold L. Bloom

SUMMARY

Mean skin-friction coefficients on a flat-plate model, with and without initial roughness, and on a wind tunnel wall were measured at a nominal Mach number of 5.5 over a Reynolds number range from lxl0⁶ to lxl0⁷, and the results were compared with analytical values. Although evidence of air condensation was obtained in the test section, experimental mean skin-friction coefficients on the tunnel wall and on the flat plate with artificial transition agreed quite well with the analytical results of H. U. Eckert and of E. R. Van Driest. Experimental skin-friction coefficients on the plate with natural transition fell between theoretical laminar values and the analytical turbulent values of Eckert and of Van Driest. Because of the presence of air condensation, the results reported herein must be regarded as tentative.

INTRODUCTION

In references 1 to 3, analytical methods are developed for predicting turbulent skin-friction coefficients at Mach numbers for which property values cannot be assumed constant through the boundary layer. At high Mach numbers, a large variation exists between the values of skin-friction coefficients given by the various methods. A need for expanding the range of experimental data on skin friction to higher Mach numbers is therefore apparent.

The purpose of this report is to present preliminary boundary-layer and skin-friction data accumulated at the NACA Lewis laboratory in a 6- by 6-inch wind tunnel with a nominal test section Mach number of 5.5. The present investigation involves three phases: surveys of the turbulent boundary layer on the bottom wall of the tunnel itself, surveys of the boundary layer on a smooth flat-plate model mounted in the test section of the tunnel, and surveys of the boundary layer on a flat-plate model with roughness added near the leading edge to induce transition of the boundary layer. Since evidence of air condensation in the test section was found, the data contained herein must be regarded as tentative until comparison with similar data for condensation-free flow becomes possible.

APPARATUS AND PROCEDURE

Model

The investigation was carried out in the 6- by 6-inch, hypersonic continuous-flow tunnel shown schematically in figure 1. A photograph of the tunnel, given in figure 2, shows the nozzle, test section, supersonic diffuser, and model in position for testing. Inlet pressures for all tests were held to 280±2 inches of mercury absolute, and inlet temperatures of 112°±10° F were maintained. The air supplied at these conditions was dried to a dew point of -45°±10° F.

Figure 3 provides a view of the plate model with a strip of roughness cemented to the leading section. The test model was machined from solid brass stock to the following dimensions: length, 16 inches; width (not including faired support section at rear), 4 inches; thickness, 0.25 inch; leading-edge angle, 15°; leading-edge thickness, about 0.006 inch.

A fully developed turbulent boundary layer with natural transition on the plate model would have required a length of plate so long as to assure contamination of the plate boundary layer by the tunnel side wall boundary layer and by the model tip effects. To hasten transition, and to avoid such contamination, a boundary-layer trip, consisting of a strip of carborundum grit, was cemented to the leading section of the model as shown in figure 3. Profile data taken with various grades and lengths of roughness indicated that the boundary layer downstream of the trip was fully turbulent when the strip was composed of number 60 grit with a length of 1 inch in the direction of the flow. The mean thickness of the trip was approximately 0.012 inch, and the closest survey point was $2\frac{5}{8}$ inches downstream of the trailing edge of the trip where there were no detectable disturbances from the roughness.

Figures 2 and 3 show the model mounted 1 inch below the center line of the tunnel. This location was chosen to avoid the possibility of disturbance of the plate boundary layer by the reflected leading-edge shock. To avoid secondary flows due to the tunnel wall boundary layer, the plate was constructed so that the side edges were 1 inch from the tunnel walls. For such models, however, the possibility exists that secondary flow around the edges from the bottom surface to the top may occur. The possible effect of secondary flow will be discussed in connection with the presentation of data.

Pressure Measurements

The probes used in this investigation are shown in figure 4. Probes A and B are total-pressure probes, and, except for length, have

almost identical tip dimensions (~0.006 by 0.040 in. 0. D.). Readings by probes A and B at the same position in the tunnel differed by less than 0.5 percent. Probe C, the static-pressure probe, consists of a 78 caliber ogival forebody with a cylindrical afterbody, and its four static orifices located 4 diameters downstream of the beginning of the cylindrical portion of the probe are spaced at 90° intervals around the circumference.

During surveys the probes were connected to a differential manometer utilizing butyl phthalate as the working fluid. The reading accuracy of this manometer system is considered to be ±0.05 inch of butyl phthalate, and a hand-operated micrometer probe actuator can position the probe with an accuracy of ±0.0005 inch.

Total-pressure profiles were obtained by surveying the boundary layer with either pitot probe A or B (fig. 4) at various axial positions on the bottom wall of the tunnel and on the flat-plate model. The process was repeated with static probe C to obtain static-pressure profiles at corresponding positions.

Tunnel Calibration

Mach number calibration profiles taken at both ends of the test section on the center line of a side wall are shown in figure 5, and static-pressure readings taken along the center line of the top and the bottom walls of the tunnel, in figure 6. The data show very little scatter; in the region outside the boundary layer, where the model was located, the flow is uniform at each axial position. There is, however, an axial Mach number variation (5.06 < M < 5.57) which will be discussed later.

At the operating conditions of this investigation the possibility of condensation exists. Criteria from reference 4 indicate border-line conditions with regard to condensation in the test section, and a light-diffusion test, as proposed in reference 5, was performed for further confirmation. A foggy beam of light appearing between the walls at the flow condition indicated that some condensation occurred. A quantitative estimate, however, is not possible.

The effect of condensation on the boundary layer may be similar to that of heat transfer, since the chief variable, if static pressure is constant, is the stagnation temperature gradient due to the probable decrease in amount of condensation as the temperature varies from the free-stream value to the surface value. Since the assumption that stagnation temperature is constant through the boundary layer yields a good approximation for friction drag even when heat transfer exists to a moderate extent, it is possible that limited amounts of condensation

may have a negligible effect on measured skin friction. Since the precise effect is as yet unknown, the data presented herein should be regarded as tentative. For the purpose of comparison of experimental and analytical results, the effect of condensation on computed skin friction and velocity profiles was assumed small.

PRESENTATION OF DATA

Velocity Profiles

In figure 7(a) is shown the Mach number distribution in the boundary layer of the tunnel wall as calculated from the total- and static-pressure surveys at each axial position. The plotted data indicate that the Mach number profiles are essentially similar for all axial positions with the maximum variation near the surface. A profile derived from the ½th power law, assuming constant total temperature and free-stream Mach number equal to 5, is shown in figure 7(a) for purposes of comparison. Except near the outer edge of the boundary layer, the agreement between the experimental profile and the power-law profile is good.

Figure 7(b) shows the Mach number profiles in the boundary layer of the plate model with roughness added and also the theoretical profile described previously. Here again the similarity of all profiles indicates that fully turbulent flow is established. There is, however, a difference in profile shape between the wall data and the plate data, which may be due to the difference in axial Mach number gradient, to the persistence of a leading-edge effect, or to a nonequilibrium of the flow associated with the added roughness.

The Mach number distributions plotted in figure 7(c) show the profiles in the boundary layer on the plate model with smooth surface. These profiles are similar in shape to an analytical laminar profile, but show only little agreement with it. The disagreement may be due to distortion of an initially laminar layer by the secondary flow mentioned previously. Since it is known from shock boundary-layer work that a laminar boundary layer is more sensitive to pressure disturbances than a turbulent boundary layer, it may be expected that the results for the plate with natural transition have been affected to a larger degree by secondary flow than the results for the plate with forced transition. The last survey point (x = 9.84 in.) is located very close to the point where disturbances from the model leading-edge tips could, by potential flow theory, contaminate the plate boundary layer. The results of this report do not include data from this last survey position.

Momentum and Displacement Thicknesses

The momentum and displacement thicknesses are defined by

$$\theta = \int_0^{\delta} \frac{\rho u}{\rho_1 u_1} \left(1 - \frac{u}{u_1} \right) dy \tag{la}$$

$$\delta^* = \int_0^{\delta} \left(1 - \frac{\rho u}{\rho_1 u_1}\right) dy \tag{1b}$$

These parameters may be expressed in terms of the local values of Mach number M and total temperature T, namely,

$$\theta = \int_{0}^{\delta} \left[\frac{M}{M_{1}} \frac{\sqrt{1 + \frac{\Upsilon - 1}{2} M^{2}}}{\sqrt{1 + \frac{\Upsilon - 1}{2} M_{1}^{2}}} \frac{\sqrt{T_{1}}}{\sqrt{T}} - \left(\frac{M}{M_{1}}\right)^{2} \right] dy$$
 (2a)

$$\delta^* = \int_0^{\delta} \left(1 - \frac{M}{M_1} \frac{\sqrt{1 + \frac{\Upsilon - 1}{2} M^2}}{\sqrt{1 + \frac{\Upsilon - 1}{2} M_1^2}} \frac{\sqrt{T_1}}{\sqrt{T}} \right) dy$$
 (2b)

For $T = T_1 = constant$, these equations become

$$\theta = \int_0^{\delta} \left[\frac{M}{M_1} \sqrt{\frac{1 + \frac{\Upsilon - 1}{2} M^2}{1 + \frac{\Upsilon - 1}{2} M_1^2}} - \left(\frac{M}{M_1}\right)^2 \right] dy$$
 (3a)

$$\delta * = \int_{0}^{\delta} \left(1 - \frac{M}{M_{1}} \sqrt{\frac{1 + \frac{\Upsilon - 1}{2} M^{2}}{1 + \frac{\Upsilon - 1}{2} M_{1}^{2}}} \right) dy$$
 (3b)

To determine the effect of assuming a constant total temperature in the boundary layer, theoretical values of θ and δ^* were computed from equations (2) for a laminar boundary layer at a Mach number of 5.5 using values of T and M based on reference 6. These values were

compared with values of θ and δ^* computed from equations (3) using the same Mach number distribution. The latter calculation agreed with the former to within 1.5 percent. This result indicates that it is sufficient to find the Mach number distribution normal to the wall in the boundary layer and to compute θ and δ^* from equations (3a) and (3b) if the total-temperature variations are of the order of those expected for laminar flow over an insulated flat plate. This procedure is used in the present report for all the boundary layers, since the total temperature in a turbulent boundary layer is expected to be more nearly constant than that in a laminar one.

Figures 8(a), 8(b), and 8(c) show the boundary-layer parameters, displacement thickness, momentum thickness, and form parameter, for the three test surfaces as calculated directly from the Mach number profiles. Included in figures 8(a) and 8(b) are theoretical values of the form parameter H as derived from reference 1. In each case there is fair agreement between measured values and theoretical points. Figure 8(c) includes theoretical values of H derived from the laminar theory of reference 6. The experimental values fall below the theoretical laminar values on the plate with natural transition, and yet are larger than turbulent values (fig. 8(b)). Also shown in figures 8(a) to 8(c) are the local Mach number distributions along each surface. In each case, changes in axial Mach number have a greater effect on the displacement thickness than on the momentum thickness. Consequently, the form parameter varies with the Mach number.

Method of Calculation

The local skin-friction coefficient c_{f} may be expressed in terms of δ^* and θ as

$$\frac{c_{f}}{2} = \frac{\tau}{\rho_{l} u_{l}^{2}} = \frac{d\theta}{dx} + \left[\frac{\left(2 - M_{l}^{2}\right) + \frac{\delta^{*}}{\theta}}{M_{l}\left(1 + \frac{\gamma - 1}{2} M_{l}^{2}\right)} \frac{dM_{l}}{dx} \right] \theta \tag{4}$$

where τ is the local shear stress and x is the axial distance from a reference leading edge.

The mean, or average, skin-friction coefficient $\text{C}_{\overline{F}}$ is related to the local shear stress τ by

$$C_{\rm F} = \frac{2}{x(\rho_{\rm R} u_{\rm R}^2)} \int_0^x \tau \, \mathrm{d}x \tag{5}$$

where the subscript R denotes constant values taken at a reference station. Hence, from equation (4),

$$C_{\mathrm{F}} = \frac{2}{x} \int_{0}^{x} \frac{\rho_{1} u_{1}^{2}}{\rho_{R} u_{R}^{2}} \left\{ \frac{d\theta}{dx} + \left[\frac{(2-M_{1}^{2}) + \frac{8*}{\theta}}{M_{1} \left(1 + \frac{\gamma-1}{2} M_{1}^{2}\right)} \frac{dM_{1}}{dx} \right] \theta \right\} dx \qquad (6)$$

The initial term in equation (4) represents the local skin-friction coefficient when the axial Mach number gradient is zero, while the second term of the equation is the contribution of the axial Mach number gradient to the friction coefficient. With ρ_R and u_R^2 evaluated at the test section entrance, equation (6) was integrated numerically to obtain values of C_F . The integration provided values of C_F which included the contribution of the axial Mach number gradient. For zero gradient the mean skin-friction coefficient becomes simply $2\theta/x$.

When an attempt is made to compare experimental and analytical variations of local or mean skin-friction coefficient with Reynolds number, consideration must be given to the fact that conditions in the experiment may not correspond to conditions assumed in the analysis. One method frequently used to compensate for some of these differences (nonzero leading-edge thickness, added roughness, laminar run) is to define an "effective leading edge," which is essentially the length of flat-plate run required to develop the momentum or displacement thickness measured at the first experimental station. This method was used to obtain an effective Reynolds number for both local and mean skin-friction coefficient calculations. Since the procedure is somewhat arbitrary, however, values of skin-friction coefficient obtained without leadingedge correction are also presented. Specifically, the procedure used to define the effective leading edge was as follows: The variation of θ with distance (figs. 8(a) to 8(c)) was extrapolated to $\theta = 0$ as a straight line having the slope of the fore part of the experimental curve. The point where the slope line crossed the $\theta = 0$ line was called the leading edge based on θ . The same procedure was carried out with the curve of δ^* against distance to reference to obtain a leading edge based on &*. The effective leading edge was then assumed to be the average of these two values. This procedure yielded an effective leading edge for the tunnel wall 16.6 inches upstream of the first survey point. Other methods are available for correcting the leading edge; reference 3, for example, presents a method which yields an effective leading-edge value 20 percent smaller than that given. However, the simplicity of the method described and the fact that it presents a limiting maximum correction were deciding factors in its adoption for the data of this investigation. The effective leading edge was located 0.91 inch upstream of the actual leading edge for the plate with artificial transition. For the results obtained with natural transition

the linear correction would have placed the effective leading edge about 5.5 inches upstream of the actual edge. Since this correction seems unreasonably large, and since the profiles obtained with natural transition were not of the usual laminar or turbulent type, only the uncorrected results for the case of natural transition will be presented.

DISCUSSION OF RESULTS

Local skin-friction coefficients. - In figure 9 are plotted experimental and theoretical values of local skin-friction coefficient against local Reynolds number. For all three test surfaces there are two values of c_f for each survey point. One is simply $2 \, d\theta/dx$, the equivalent of a flat-plate flow calculation; whereas the other was found from equation (4) and includes the Mach number gradient term. The value of $d\theta/dx$ in each case was obtained graphically from faired curves of against x (fig. 8). Since in some cases more than one curve may be faired through the given data points, the fairing used for calculations is not presented in the figures. The difference in results from reasonable fairings, however, is small. For the two cases of the plate model the experimental points include calculations based on both effective and actual leading edges.

The theoretical curves of figure 9 are based on calculations from references 1, 2, 6, and 7. In reference 1, the results of pipe tests are applied to obtain the characteristics of the compressible turbulent boundary layer on a flat plate. The resulting equation for local skin-friction coefficient is

$$c_{f} = 0.0944\Theta \left(\frac{\overline{T}}{\overline{T}_{U}}\right)^{-\frac{3-\omega}{5}} - \frac{1}{5}$$
 Re (7)

where Re is the Reynolds number, and Θ , \overline{T}/T_U , and ω are parameters derived from reference 1. Values of Θ and \overline{T}/T_U are shown graphically in reference 1 for various values of M and n. A value of n = 7 is assumed in this report, and the assumption of ω = 1 is reasonable for the temperature range of the test tunnel.

In reference 2, the Prandtl incompressible-fluid wall formula is modified by allowing the density to vary. The resulting local skin-friction law based on stream conditions is then given as

$$c_{f} = \frac{0.558(1-\lambda^{2})^{\frac{1}{2}} \frac{\sin^{-1} \lambda}{\lambda} c_{F}}{0.558(1-\lambda^{2})^{\frac{1}{2}} \frac{\sin^{-1} \lambda}{\lambda} + 2c_{F}^{\frac{1}{2}}}$$
(8)

where λ is a function of Mach number, and C_F , the mean skin-friction coefficient, will be discussed in the following section.

The skin-friction coefficients from equations (7) and (8) are plotted in figure 9 for Mach numbers 5 and 6, and show that relatively slight changes of cf with M should be expected when no pressure gradient exists. As a lower limit for turbulent theories, von Karman's estimation from reference 7 is plotted in figure 9.

The curve for laminar skin-friction coefficient in figure 9 was calculated from equations of reference 6, from which, if the wall temperature is assumed constant, there is obtained

$$c_{f} = \frac{0.664 \sqrt{C}}{\sqrt{Re}}$$
 (9)

For the range of this experiment C, as calculated by the method of reference 6, is very nearly equal to 1.

The experimental values of c_f for the plate with artificial transition and for the tunnel wall are generally larger than the values predicted by the analyses of references 1 and 2, although those analyses give higher values than other compressible turbulent boundary-layer analyses. The experimental points on the plate with natural transition generally fall between curves of turbulent theory and laminar theory.

Although the experimental points of figure 9 show a large amount of scatter in general, inspection of that data in conjunction with figures 8(a) to 8(c) indicates that there is a tendency for the local skin-friction coefficient to increase in a negative axial Mach number gradient and to decrease in a positive axial Mach number gradient.

The leading-edge correction is relatively small, and the correction term in equation (4) for the effect of pressure gradient appears to be inadequate to account for the relatively large changes obtained experimentally.

Mean skin-friction coefficients. - Since mean or average skin-friction coefficients depend chiefly on local velocity profiles rather than on slopes of curves through scattered points, they may be more reliable, from the standpoint of experimental accuracy, than local skin-friction coefficients. Values of $C_{\rm F}$ obtained in this investigation are plotted in figure 10. For each point there are plotted both the equivalent flat-plate values $2\theta/x$ and the values including the contribution of the Mach number gradient, which were obtained from equation (6).

The theoretical curves of figure 10 are derived from references 1, 2, 6, and 7. In reference 1, the expression obtained for the mean skin-friction coefficient is

$$C_{\rm F} = 0.118\Theta^{\frac{1}{5}} \left(\frac{\overline{T}}{T_{\rm U}}\right)^{-\frac{3-\omega}{5}} = \frac{1}{5}$$
 (10)

where the values of Θ , \overline{T}/T_U , and ω are found in the same manner as for the local skin-friction coefficient.

In reference 2, an equation is derived for mean skin-friction coefficient which is based on the power viscosity law $\mu/\mu_1 = (t/t_1)^{\omega}$. For the skin-friction coefficient based on free-stream conditions,

$$\frac{0.242}{c_{\rm F}^{\frac{1}{2}}} (1-\lambda^2)^{\frac{1}{2}} \frac{\sin^{-1} \lambda}{\lambda} = \log (\text{Re } c_{\rm F}) + \frac{1+2\omega}{2} \log (1-\lambda^2)$$
 (11)

where λ is, as for the local skin-friction coefficient, a function of Mach number, Re is the Reynolds number based on length, and ω is the viscosity power law parameter. For the conditions of this investigation, ω is assumed equal to 1. The value of C_F as calculated from equation (11) is used in the computation of c_f in equation (8).

To present a possible lower limit of turbulent mean skin-friction coefficient, there is plotted in figure 10 a curve from reference 7, in which an estimate is presented for extending an incompressible fluid formula to the compressible case. This approximation is

$$\frac{0.242}{\sqrt{C_{\rm F}}} \left(1 + \frac{\gamma - 1}{2} \, M_{\rm L}^2\right)^{\frac{1}{2}} = \log \left(\text{Re } C_{\rm F}\right) - \frac{1}{2} \log \left(1 + \frac{\gamma - 1}{2} \, M_{\rm L}^2\right) \tag{12}$$

Finally, the theoretical laminar mean skin-friction coefficient from reference 6 is plotted in figure 10. The expression may be written

$$C_{\rm F} = \frac{1.328}{\sqrt{\rm Re}} \sqrt{C} \tag{13}$$

Except for the Mach number gradient effects, the experimental values of turbulent mean skin-friction coefficient plotted in figure 10 for the tunnel wall and for artificial transition show fair agreement with the analyses of reference 1 or reference 2. The observed scatter about the theoretical curves for the artificial transition case appears to be of the same magnitude as the variation caused by the leading-edge correction.

In addition, inspection of figures 10 and 8(b) indicates that the observed divergence of experimental mean skin-friction coefficient from the theoretical as Reynolds number increases may be associated with the general decrease in Mach number along the plate.

The data from the plate with natural transition are in the turbulent value region, but the slope of a line through that data is approximately equal to the slope of the theoretical laminar values, which is 1/2. Thus, no conclusions can be drawn from the data of the plate without roughness.

It can be concluded from the turbulent boundary-layer results presented in figure 10 that for the boundary layers on the wall and on the plate model with initial roughness, the experimental mean skin-friction coefficients at $M \approx 5.5$ agree quite well with the analytical values given in references 1 and 2, even though there was some air condensation present in the test section.

SUMMARY OF RESULTS

Measurements in the boundary layer on a tunnel wall and on a flat plate with artificial transition at a Mach number of about 5.5 and Reynolds numbers of from 1×10^6 to 1×10^7 yielded turbulent mean skinfriction coefficients which agreed quite well with those predicted by the analyses of Eckert and of Van Driest, even though evidence of air condensation was found in the test section. The measured point-to-point variation of skin-friction coefficients appeared to be larger than that indicated by the conventional pressure gradient correction term in the momentum equation.

Mach number profiles measured on a flat plate with natural transition were not in agreement with theoretical laminar or turbulent profiles. Friction coefficients obtained from these experimental profiles were intermediate between theoretical laminar values and values of the turbulent theories of Eckert and of Van Driest.

Lewis Flight Propulsion Laboratory
National Advisory Committee for Aeronautics
Cleveland, Ohio

APPENDIX - SYMBOLS

The following symbols are used in this report:

- C factor of proportionality in viscosity variation law, $\frac{\mu}{\mu_1} = C \frac{t}{t_1}$
- CF mean skin-friction coefficient
- cf local skin-friction coefficient
- M Mach number
- n exponent of velocity distribution power law
- Po inlet total pressure
- p static pressure
- Rex local stream Reynolds number
- T total temperature
- t static temperature
- $\frac{\overline{T}}{T_U}$ ratio of temperature of mean mass flow to temperature at pipe center, reference 1
- u local velocity
- x distance from reference in direction of air flow
- y normal distance from solid boundary
- γ ratio of specific heats of air
- δ boundary-layer thickness
- δ* displacement thickness
- Θ ratio of momentum thickness to boundary-layer thickness, θ/δ
- θ momentum thickness
- λ Mach number function = $\sqrt{\frac{\frac{\Upsilon-1}{2} M_1^2}{1 + \frac{\Upsilon-1}{2} M_1^2}}$, reference 2

- μ dynamic viscosity of air
- ρ density
- τ shear stress at wall
- exponent of viscosity variation power law, $\frac{\mu}{\mu_1} = \left(\frac{t}{t_1}\right)^{\omega}$, reference 1

Subscripts:

- l conditions at outer edge of boundary layer
- R conditions at reference station at entrance to test section

REFERENCES

- 1. Eckert, Hans Ulrich: Characteristics of the Turbulent Boundary Layer on a Flat Plate in Compressible Flow from Measurements of Friction in Pipes. Jour. Aero. Sci., vol. 17, no. 9, Sept. 1950, pp. 573-584.
- 2. Van Driest, E. R.: Turbulent Boundary Layer for Compressible Fluids on an Insulated Flat Plate. Rep. AL-958, Proj. MX-770, Aerophysics Lab., North American Aviation, Inc., Sept. 15, 1949.
- 3. Rubesin, Morris W., Maydew, Randall C., and Varga, Steven A.: An Analytical and Experimental Investigation of the Skin Friction of the Turbulent Boundary Layer on a Flat Plate at Supersonic Speeds. NACA TN 2305, 1951.
- 4. Stever, H. Guyford, and Rathbun, Kenneth C.: Theoretical and Experimental Investigation of Condensation of Air in Hypersonic Wind Tunnels. NACA TN 2559, 1951.
- 5. Wegener, P., Stollenwerk, E., Reed, S., and Lundquist, G.: NOL Hyper-ballistics Tunnel No. 4 Results I: Air Liquefaction. NAVORD Rep. 1742, Aeroballistic Res. Rep. 19, U.S. Naval Ordnance Lab., Jan. 4, 1951.
- 6. Chapman, Dean R., and Rubesin, Morris W.: Temperature and Velocity Profiles in the Compressible Laminar Boundary Layer with Arbitrary Distribution of Surface Temperature. Jour. Aero. Sci., vol. 16, no. 9, Sept. 1949, pp. 547-565.
- 7. de Kármán, Th.: The Problem of Resistance in Compressible Fluids.
 Quinto Convegno "Volta," Reale Accademia d'Italia (Roma), Sett.
 30 Ott. 6, 1935, pp. 3-57.

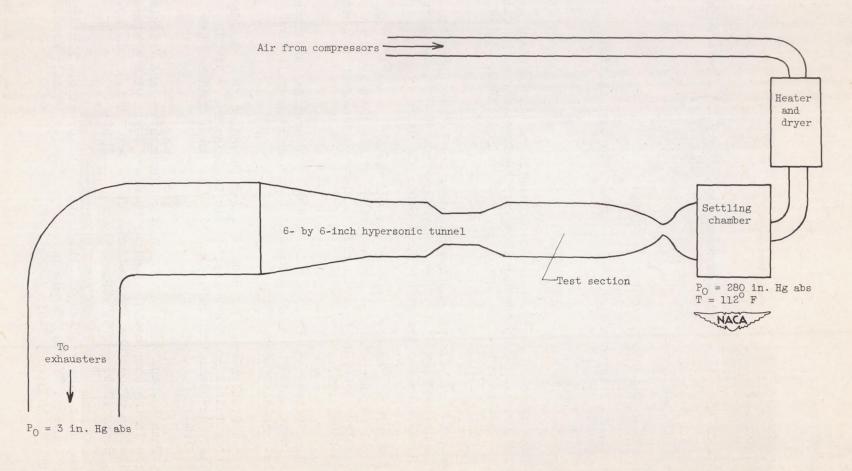


Figure 1. - Schematic diagram of 6- by 6-inch hypersonic tunnel.

15

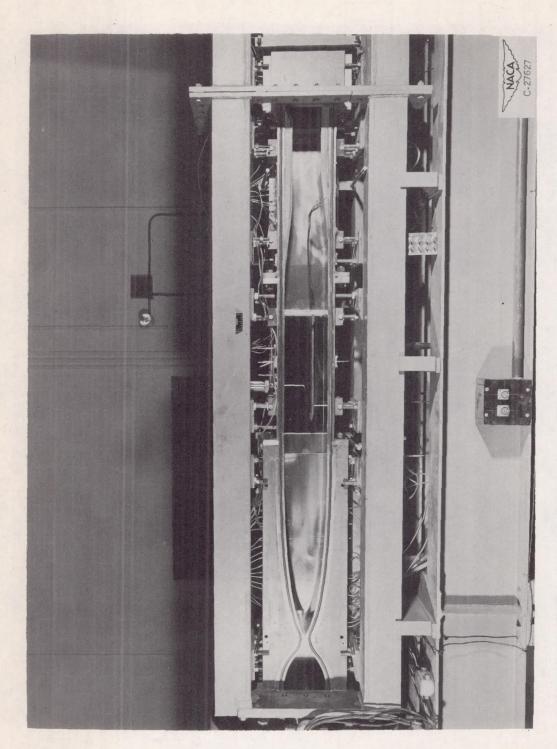


Figure 2. - View of tunnel with model in test section.

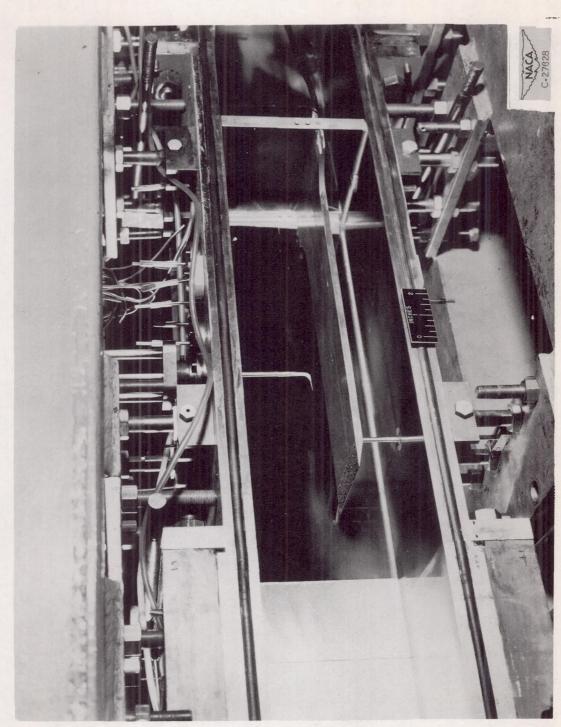


Figure 3. - Model with roughness.

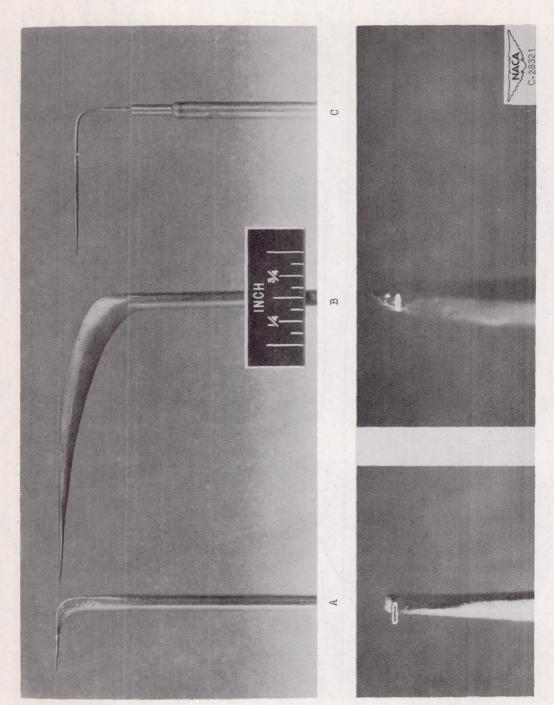


Figure 4. - Boundary-layer survey probes.

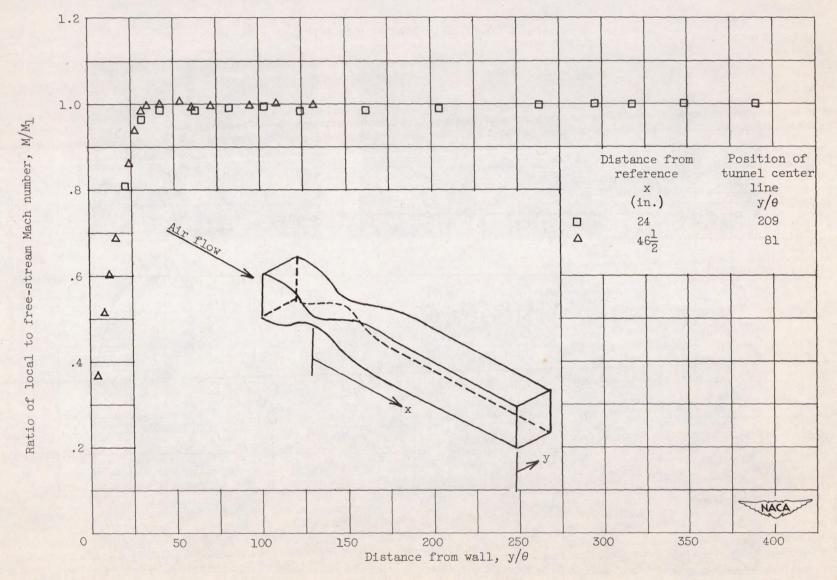


Figure 5. - Calibration surveys across tunnel.

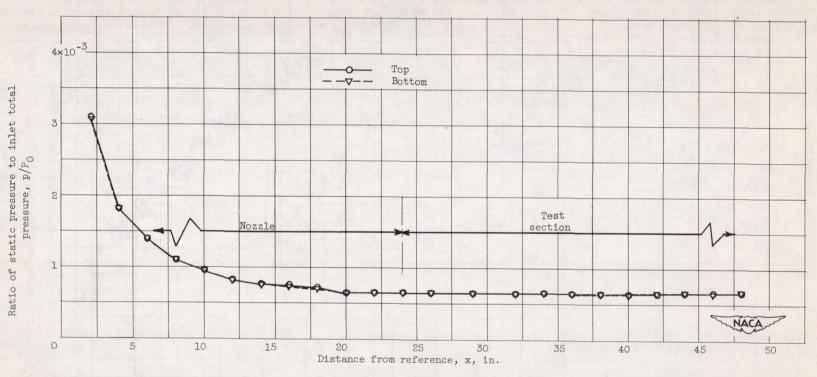


Figure 6. - Static-pressure distribution along tunnel.

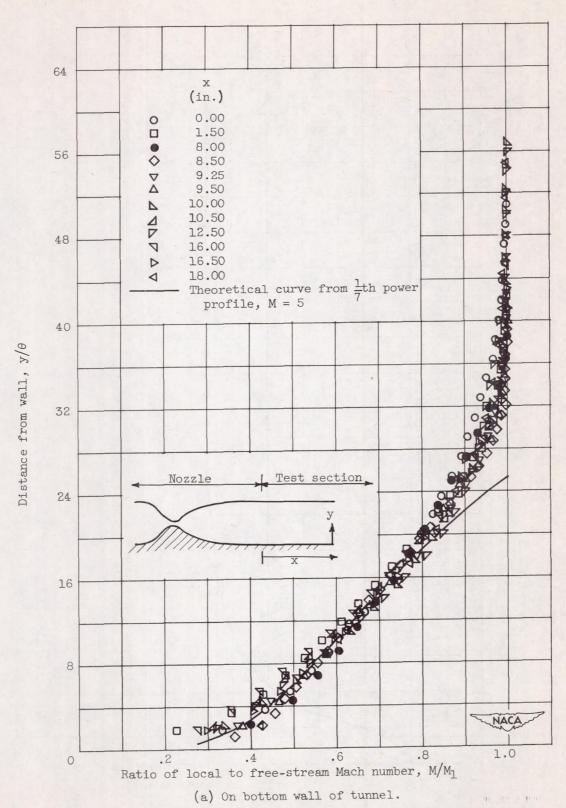


Figure 7. - Mach number in boundary layer.

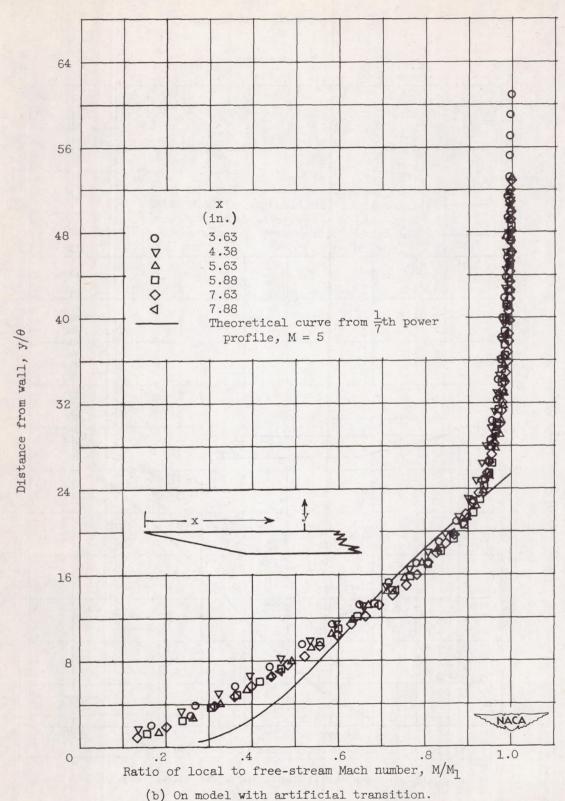
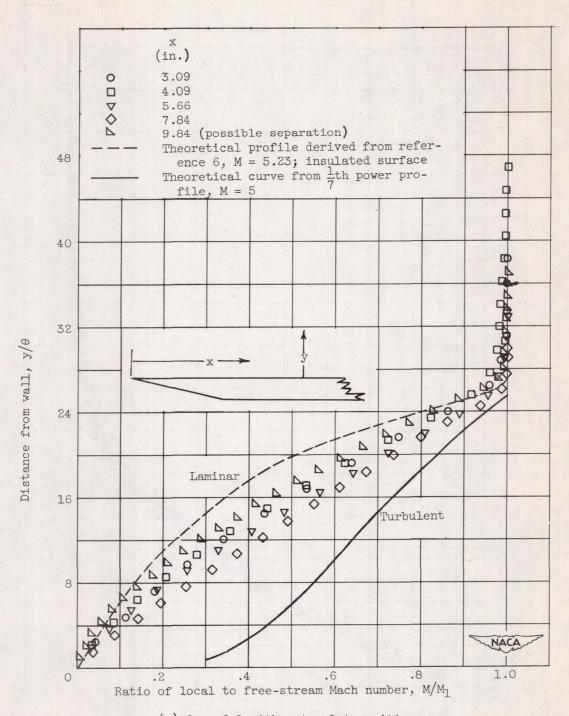


Figure 7. - Continued. Mach number in boundary layer.



(c) On model with natural transition.

Figure 7. - Concluded. Mach number in boundary layer.

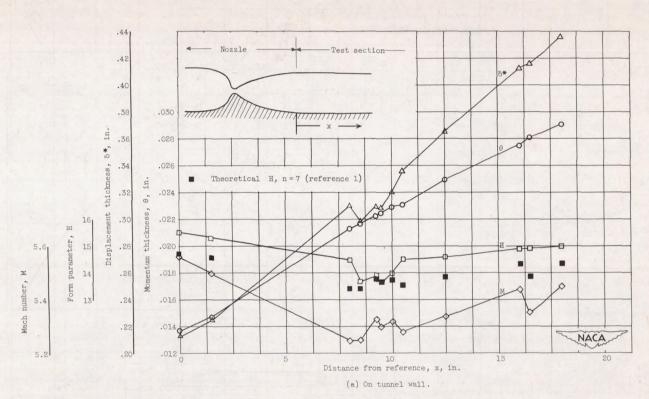


Figure 8. - Boundary-layer measurements.

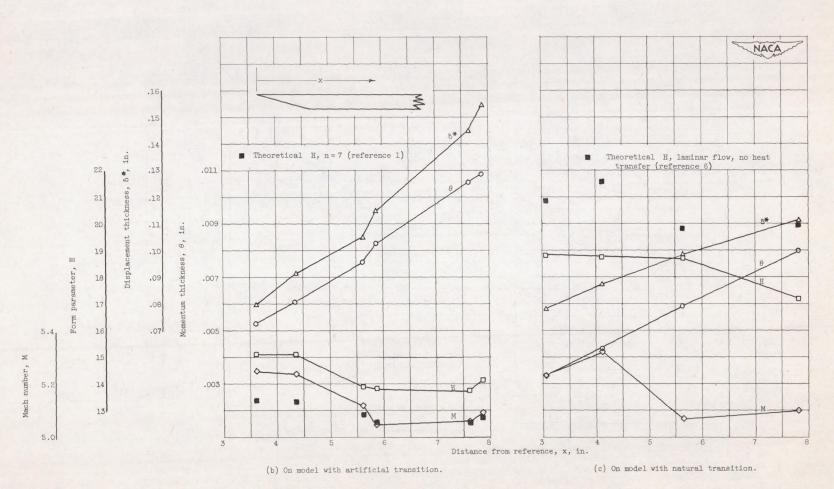


Figure 8. - Concluded. Boundary-layer measurements.

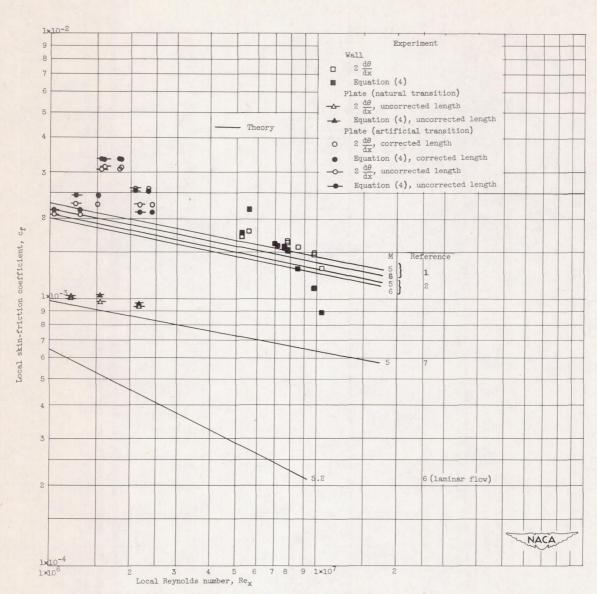


Figure 9. - Local skin-friction coefficient.

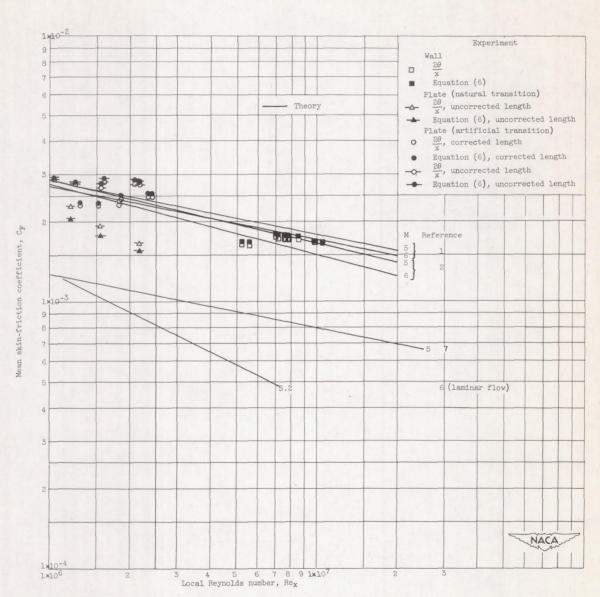


Figure 10. - Mean skin-friction coefficient.